

Moments of the Hadronic Invariant Mass Spectrum in $B \rightarrow X_c \ell \nu$ Decays at Belle

C. Schwanda,¹¹ K. Abe,⁸ I. Adachi,⁸ H. Aihara,⁴⁵ D. Anipko,¹ V. Aulchenko,¹
 E. Barberio,²¹ A. Bay,¹⁸ I. Bedny,¹ K. Belous,¹² U. Bitenc,¹⁴ I. Bizjak,¹⁴ A. Bondar,¹
 A. Bozek,²⁷ M. Bračko,^{8,20,14} T. E. Browder,⁷ P. Chang,²⁶ A. Chen,²⁴ W. T. Chen,²⁴
 B. G. Cheon,³ R. Chistov,¹³ Y. Choi,³⁹ Y. K. Choi,³⁹ S. Cole,⁴⁰ J. Dalseno,²¹ M. Dash,⁴⁸
 S. Eidelman,¹ S. Fratina,¹⁴ N. Gabyshev,¹ T. Gershon,⁸ A. Go,²⁴ G. Gokhroo,⁴¹
 B. Golob,^{19,14} H. Ha,¹⁶ J. Haba,⁸ M. Hazumi,⁸ D. Heffernan,³² Y. Hoshi,⁴³ S. Hou,²⁴
 W.-S. Hou,²⁶ T. Iijima,²² K. Ikado,²² K. Inami,²² A. Ishikawa,⁴⁵ R. Itoh,⁸ M. Iwasaki,⁴⁵
 Y. Iwasaki,⁸ J. H. Kang,⁴⁹ S. U. Kataoka,²³ N. Katayama,⁸ H. Kawai,² T. Kawasaki,²⁹
 H. R. Khan,⁴⁶ H. Kichimi,⁸ Y. J. Kim,⁶ K. Kinoshita,⁴ P. Križan,^{19,14} P. Krokovny,⁸
 R. Kumar,³³ C. C. Kuo,²⁴ Y.-J. Kwon,⁴⁹ J. S. Lange,⁵ M. J. Lee,³⁷ S. E. Lee,³⁷ T. Lesiak,²⁷
 A. Limosani,⁸ S.-W. Lin,²⁶ D. Liventsev,¹³ J. MacNaughton,¹¹ G. Majumder,⁴¹ F. Mandl,¹¹
 T. Matsumoto,⁴⁷ A. Matyja,²⁷ S. McOnie,⁴⁰ W. Mitaroff,¹¹ H. Miyake,³² H. Miyata,²⁹
 Y. Miyazaki,²² R. Mizuk,¹³ G. R. Moloney,²¹ T. Mori,²² T. Nagamine,⁴⁴ E. Nakano,³¹
 M. Nakao,⁸ Z. Natkaniec,²⁷ S. Nishida,⁸ T. Nozaki,⁸ T. Ohshima,²² S. Okuno,¹⁵
 Y. Onuki,³⁵ H. Ozaki,⁸ P. Pakhlov,¹³ G. Pakhlova,¹³ C. W. Park,³⁹ H. Park,¹⁷ L. S. Peak,⁴⁰
 R. Pestotnik,¹⁴ L. E. Pilonen,⁴⁸ Y. Sakai,⁸ N. Satoyama,³⁸ T. Schietinger,¹⁸ O. Schneider,¹⁸
 R. Seidl,^{9,35} K. Senyo,²² M. E. Sevier,²¹ M. Shapkin,¹² H. Shibuya,⁴² J. B. Singh,³³
 A. Somov,⁴ N. Soni,³³ S. Stanič,³⁰ M. Starič,¹⁴ H. Stoeck,⁴⁰ T. Sumiyoshi,⁴⁷ S. Y. Suzuki,⁸
 F. Takasaki,⁸ K. Tamai,⁸ M. Tanaka,⁸ G. N. Taylor,²¹ Y. Teramoto,³¹ X. C. Tian,³⁴
 I. Tikhomirov,¹³ K. Trabelsi,⁷ T. Tsuboyama,⁸ T. Tsukamoto,⁸ S. Uehara,⁸ T. Uglov,¹³
 S. Uno,⁸ P. Urquijo,²¹ Y. Usov,¹ G. Varner,⁷ K. E. Varvell,⁴⁰ S. Villa,¹⁸ C. H. Wang,²⁵
 M.-Z. Wang,²⁶ Y. Watanabe,⁴⁶ E. Won,¹⁶ Q. L. Xie,¹⁰ B. D. Yabsley,⁴⁰ A. Yamaguchi,⁴⁴
 Y. Yamashita,²⁸ M. Yamauchi,⁸ L. M. Zhang,³⁶ Z. P. Zhang,³⁶ V. Zhilich,¹ and A. Zupanc¹⁴

(The Belle Collaboration)

¹*Budker Institute of Nuclear Physics, Novosibirsk*

²*Chiba University, Chiba*

³*Chonnam National University, Kwangju*

⁴*University of Cincinnati, Cincinnati, Ohio 45221*

⁵*University of Frankfurt, Frankfurt*

⁶*The Graduate University for Advanced Studies, Hayama, Japan*

⁷*University of Hawaii, Honolulu, Hawaii 96822*

⁸*High Energy Accelerator Research Organization (KEK), Tsukuba*

⁹*University of Illinois at Urbana-Champaign, Urbana, Illinois 61801*

¹⁰*Institute of High Energy Physics,*

Chinese Academy of Sciences, Beijing

¹¹*Institute of High Energy Physics, Vienna*

¹²*Institute of High Energy Physics, Protvino*

¹³*Institute for Theoretical and Experimental Physics, Moscow*

¹⁴*J. Stefan Institute, Ljubljana*

- ¹⁵*Kanagawa University, Yokohama*
¹⁶*Korea University, Seoul*
¹⁷*Kyungpook National University, Taegu*
¹⁸*Swiss Federal Institute of Technology of Lausanne, EPFL, Lausanne*
¹⁹*University of Ljubljana, Ljubljana*
²⁰*University of Maribor, Maribor*
²¹*University of Melbourne, Victoria*
²²*Nagoya University, Nagoya*
²³*Nara Women's University, Nara*
²⁴*National Central University, Chung-li*
²⁵*National United University, Miao Li*
²⁶*Department of Physics, National Taiwan University, Taipei*
²⁷*H. Niewodniczanski Institute of Nuclear Physics, Krakow*
²⁸*Nippon Dental University, Niigata*
²⁹*Niigata University, Niigata*
³⁰*University of Nova Gorica, Nova Gorica*
³¹*Osaka City University, Osaka*
³²*Osaka University, Osaka*
³³*Panjab University, Chandigarh*
³⁴*Peking University, Beijing*
³⁵*RIKEN BNL Research Center, Upton, New York 11973*
³⁶*University of Science and Technology of China, Hefei*
³⁷*Seoul National University, Seoul*
³⁸*Shinshu University, Nagano*
³⁹*Sungkyunkwan University, Suwon*
⁴⁰*University of Sydney, Sydney NSW*
⁴¹*Tata Institute of Fundamental Research, Bombay*
⁴²*Toho University, Funabashi*
⁴³*Tohoku Gakuin University, Tagajo*
⁴⁴*Tohoku University, Sendai*
⁴⁵*Department of Physics, University of Tokyo, Tokyo*
⁴⁶*Tokyo Institute of Technology, Tokyo*
⁴⁷*Tokyo Metropolitan University, Tokyo*
⁴⁸*Virginia Polytechnic Institute and State University, Blacksburg, Virginia 24061*
⁴⁹*Yonsei University, Seoul*

Abstract

We present a measurement of the hadronic invariant mass squared (M_X^2) spectrum in charmed semileptonic B meson decays $B \rightarrow X_c \ell \nu$ based on 140 fb^{-1} of Belle data collected near the $\Upsilon(4S)$ resonance. We determine the first, the second central and the second non-central moments of this spectrum for lepton energy thresholds ranging between 0.7 and 1.9 GeV. Full correlations between these measurements are evaluated.

PACS numbers: 12.15.Hh,14.40.Nd,13.25.Hw

I. INTRODUCTION

Inclusive semileptonic decays of B mesons to charmed final states provide an avenue for measuring the Cabibbo-Kobayashi-Maskawa (CKM) matrix element $|V_{cb}|$ [1] and for determining non-perturbative hadronic properties of the B meson. In particular, the moments of the hadronic mass in $B \rightarrow X_c \ell \nu$ decays calculated in the framework of the Operator Product Expansion (OPE) and the Heavy Quark Effective Theory (HQET) [2, 3, 4, 5] depend on the b -quark mass (m_b) and a few non-perturbative matrix elements that also appear in the expression of the total semileptonic width. Thus, measurements of the hadronic invariant mass moments [6, 7, 8, 9] allow the determination of these non-perturbative parameters from the data and reduce the theoretical uncertainty in the extraction of $|V_{cb}|$ from measurements of the semileptonic branching fraction. An improved knowledge of m_b also results in a more precise determination of $|V_{ub}|$ from inclusive charmless semileptonic B decays.

This analysis uses $\Upsilon(4S) \rightarrow B\bar{B}$ events in which the hadronic decay of one B meson is fully reconstructed. The semileptonic decay of the other B is inferred from the presence of an identified lepton (electron or muon) amongst the remaining particles in the event. We calculate the first two moments of the hadronic invariant mass squared (M_X^2) distribution [10] directly from the measured spectrum after the effects of finite detector resolution have been removed using the Singular Value Decomposition algorithm [11].

The measurement described in this paper improves the results previously reported by the BaBar and CLEO collaborations [6, 7]. The sensitivity to m_b and other non-perturbative parameters is increased by lowering the minimum lepton energy threshold to 0.7 GeV. Finally, this analysis minimizes the dependence on particular $B \rightarrow X_c \ell \nu$ model assumptions by calculating the moments directly from the unfolded M_X^2 spectrum.

II. EXPERIMENTAL PROCEDURE

A. Data Sample and Event Selection

The data used in this analysis were taken with the Belle detector [12] at the KEKB asymmetric energy e^+e^- collider [13]. Belle is a large-solid-angle magnetic spectrometer that consists of a three-layer silicon vertex detector, a 50-layer central drift chamber (CDC), an array of aerogel threshold Čerenkov counters (ACC), a barrel-like arrangement of time-of-flight scintillation counters (TOF), and an electromagnetic calorimeter comprised of CsI(Tl) crystals (ECL) located inside a super-conducting solenoid coil that provides a 1.5 T magnetic field. An iron flux-return located outside of the coil is instrumented to detect K_L^0 mesons and to identify muons (KLM).

The data sample consists of 140 fb^{-1} taken near the $\Upsilon(4S)$ resonance, or 152×10^6 $B\bar{B}$ events. Another 15 fb^{-1} taken at 60 MeV below the resonance are used to estimate the non- $B\bar{B}$ (continuum) background. The off-resonance data is scaled by the integrated on- to off-resonance luminosity ratio corrected for the $1/s$ dependence of the $q\bar{q}$ cross-section.

A generic $B\bar{B}$ Monte Carlo (MC) sample equivalent to about three times the integrated luminosity is used in this analysis. MC-simulated events are generated with EvtGen [14] and full detector simulation based on GEANT3 [15] is applied. The decays $B \rightarrow D^* \ell \nu$ and $B \rightarrow D \ell \nu$ are generated using an HQET inspired form factor parameterization [16]. The decays $B \rightarrow D^{**} \ell \nu$ [17] are simulated according to the Leibovich-Ligeti-Stewart-Wise (LLSW) model [18] (both relative abundance and form factor shape). The $B \rightarrow X_c \ell \nu$ model

also includes non-resonant $B \rightarrow D^{(*)}\pi\ell\nu$ decays which are generated using the Goity-Roberts model [19]. The model for the $B \rightarrow X_u\ell\nu$ background is a hybrid mixture of exclusive modes and an inclusive component described by the De Fazio-Neubert model [20]. Light-cone sum rule form factors [21, 22] are used for $B \rightarrow \pi\ell\nu$, $\rho\ell\nu$ and $\omega\ell\nu$. Other exclusive modes are simulated according to the ISGW2 model [23]. QED bremsstrahlung in $B \rightarrow X\ell\nu$ decays is included using the PHOTOS package [24].

Hadronic events are selected based on the charged track multiplicity and the visible energy in the calorimeter. The selection is described in detail elsewhere [25].

B. Full-reconstruction Tag

We fully reconstruct the hadronic decay of one B meson (B_{tag}) using the decay modes $B^+ \rightarrow \bar{D}^{(*)0}\pi^+$, $\bar{D}^{(*)0}\rho^+$, $\bar{D}^{(*)0}a_1^+$ and $B^0 \rightarrow D^{(*)-}\pi^+$, $D^{(*)-}\rho^+$, $D^{(*)-}a_1^+$ [26]. Pairs of photons satisfying $E_\gamma > 50$ MeV in the laboratory-frame and $118 \text{ MeV}/c^2 < M(\gamma\gamma) < 150 \text{ MeV}/c^2$ ($\pm 3.3\sigma$ around the π^0 mass) are combined to form π^0 candidates. K_S^0 mesons are reconstructed from pairs of oppositely charged tracks with invariant mass within $\pm 30 \text{ MeV}/c^2$ ($\pm 5.1\sigma$) of the nominal K_S^0 mass and a decay vertex displaced from the interaction point. Candidate ρ^+ and ρ^0 mesons are reconstructed in the $\pi^+\pi^0$ and $\pi^+\pi^-$ decay modes, requiring their invariant masses to be within $\pm 150 \text{ MeV}/c^2$ of the nominal ρ mass. Candidate a_1^+ mesons are obtained by combining a ρ^0 candidate with a charged pion and requiring an invariant mass between 1.0 and 1.6 GeV/c^2 . D^0 candidates are searched for in the $K^-\pi^+$, $K^-\pi^+\pi^0$, $K^-\pi^+\pi^+\pi^-$, $K_S^0\pi^+\pi^-$ and $K_S^0\pi^0$ decay modes. The $K^-\pi^+\pi^+$ and $K_S^0\pi^+$ modes are used to reconstruct D^+ mesons. Charmed mesons are selected in a window corresponding to ± 3 times the mass resolution in the respective decay mode. D^{*+} mesons are reconstructed by pairing a charmed meson with a low momentum pion, $D^{*+} \rightarrow D^0\pi^+$, $D^+\pi^0$. The decay modes $D^{*0} \rightarrow D^0\pi^0$ and $D^{*0} \rightarrow D^0\gamma$ are used to search for neutral charmed vector mesons.

For each B_{tag} candidate, the beam-energy constrained mass M_{bc} and the energy difference ΔE are calculated,

$$M_{\text{bc}} = \sqrt{(E_{\text{beam}})^2 - (\vec{p}_B)^2}, \quad \Delta E = E_B - E_{\text{beam}}, \quad (1)$$

where E_{beam} , \vec{p}_B and E_B are the beam energy, the 3-momentum and the energy of the B candidate in the $\Upsilon(4S)$ frame. In M_{bc} and ΔE , the signal peaks at the nominal B mass and zero, respectively. We define the signal region by the selections $M_{\text{bc}} > 5.27 \text{ GeV}/c^2$ and $|\Delta E| < 0.05 \text{ GeV}$. If multiple candidates are found in a single event, the best candidate is chosen based on the proximity of ΔE , M_D and ΔM to their nominal values, where M_D is the reconstructed D meson mass and ΔM is the difference between the reconstructed D^* and D meson masses. Without making any requirement on the decay of the other B meson, the number of B^+ (B^0) tags in this region, after subtraction of continuum and combinatorial backgrounds, is $61,365 \pm 531$ ($41,027 \pm 368$), Fig. 1.

C. Lepton Reconstruction

Semileptonic decays of the other B meson (B_{signal}) are selected by searching for an identified charged lepton (electron or muon) within the remaining particles in the event. Electron candidates are identified using the ratio of the energy detected in the ECL to the track

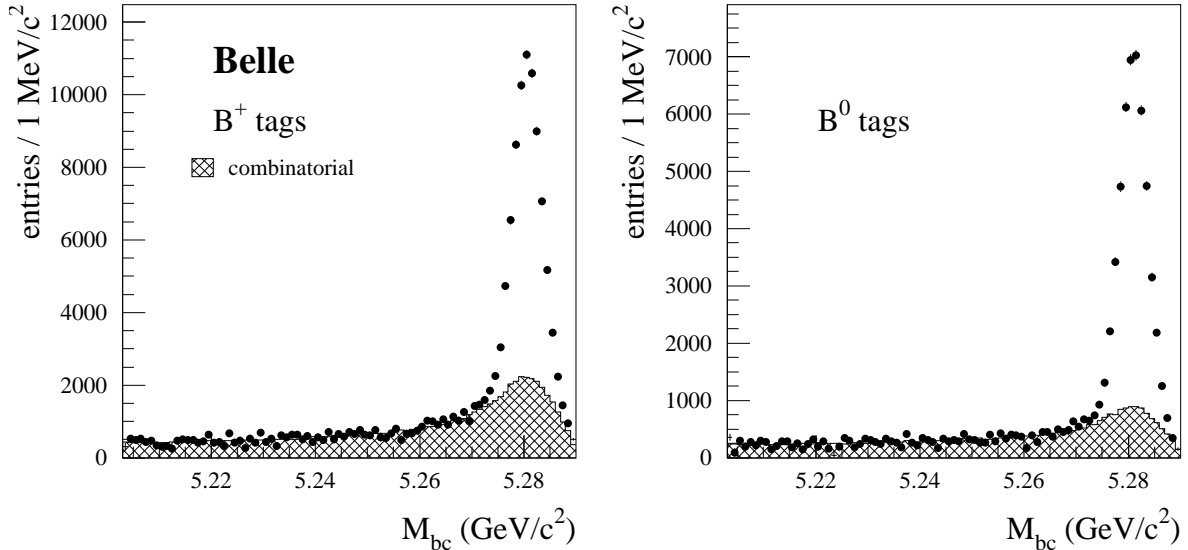


FIG. 1: M_{bc} distributions for charged and neutral B_{tag} candidates after requiring $|\Delta E| < 0.05$ GeV. No constraints are made on the signal side. The points with error bars are on-resonance data after subtraction of the scaled off-resonance data. The combinatorial background (cross-hatched histogram) is estimated using MC simulation.

momentum, the ECL shower shape, position matching between track and ECL cluster, the energy loss in the CDC and the response of the ACC counters. Muons are identified based on their penetration range and transverse scattering in the KLM detector. In the momentum region relevant to this analysis, charged leptons are identified with an efficiency of about 90% and the probability to misidentify a pion as an electron (muon) is 0.25% (1.4%) [27, 28].

We further require electron (muon) candidates to originate from near the interaction vertex, have a laboratory-frame momentum greater than 0.3 GeV/ c (0.6 GeV/ c) and satisfy $17^\circ < \theta < 150^\circ$ ($25^\circ < \theta < 145^\circ$), where θ is the polar angle in the laboratory-frame relative to the beam direction. If more than one charged lepton candidate is found in the event, we only keep the one with the highest momentum in the B rest frame. Electrons from photon conversion are vetoed by rejecting the event if the invariant mass of the electron candidate and another oppositely charged particle in the event is below 0.04 GeV/ c^2 and secondary vertex criteria are satisfied. If the charged lepton candidate is consistent with the decay $J/\psi \rightarrow \ell^+ \ell^-$ (*i.e.*, the invariant mass of the lepton candidate and another oppositely charged lepton in the event is between 3 GeV/ c^2 and 3.15 GeV/ c^2), the event is also rejected.

In B^+ tagged events, we require the lepton charge to be consistent with a prompt semileptonic decay of B_{signal} . In B^0 events, we make no requirement on the lepton charge. In electron events, we partially recover the effect of bremsstrahlung by searching for a photon with laboratory-frame energy $E_\gamma < 1$ GeV within a 5° cone around the electron direction at the interaction point. If such a photon is found, it is merged with the electron and removed from the event.

D. Hadronic Mass Reconstruction

The 4-momentum p_X of the hadronic system X recoiling against $\ell\nu$ is determined by summing the 4-momenta of the remaining charged tracks and unmatched clusters in the event. We exclude tracks passing very far away from the interaction point or compatible with a multiply reconstructed track generated by a low-momentum particle spiraling in the central drift chamber. Unmatched clusters in the barrel region must have an energy greater than 50 MeV. Higher thresholds are applied in the endcap regions.

To improve the resolution in M_X^2 , we reject events with a missing mass larger than $3 \text{ GeV}^2/c^4$. Further improvement is obtained by recalculating the 4-momentum of the X system,

$$p'_X = (p_{e^+ \text{-beam}} + p_{e^- \text{-beam}}) - p_{B_{\text{tag}}} - p_\ell - p_\nu, \quad (2)$$

taking the neutrino 4-momentum (E_ν, \vec{p}_ν) to be $(|\vec{p}_{\text{miss}}|, \vec{p}_{\text{miss}})$, where \vec{p}_{miss} is the missing 3-momentum. Defined as the half width at half maximum, the resolution in M_X^2 obtained from p'_X is about $0.8 \text{ GeV}^2/c^4$, compared to $1.4 \text{ GeV}^2/c^4$ in M_X^2 from p_X .

E. Backgrounds in the Hadronic Mass Spectrum

We consider the following contributions to the background in the M_X^2 spectrum: non- $B\bar{B}$ (continuum) background, combinatorial background, background from secondary or fake leptons and $B \rightarrow X_u \ell \nu$ background. Combinatorial background are true $B\bar{B}$ events for which reconstruction or flavor assignment of the tagged B meson is not correct.

The shapes of these background components in M_X^2 are determined from the MC simulation, except for the continuum where off-resonance data is used. The shape of the fake muon background is corrected by the ratio of the pion fake rate in the experimental data over the same quantity in the MC simulation, as measured using kinematically identified pions in $K_S^0 \rightarrow \pi^+ \pi^-$ decays. We derive the shape of the combinatorial background from the generic $B\bar{B}$ simulation by selecting events in which the reconstruction of B_{tag} does not correspond precisely to what was generated in the simulation.

The continuum background is scaled by the integrated on- to off-resonance luminosity ratio, taking into account the cross-section difference. The MC-prediction of the combinatorial background is normalized to the data using the side-band region ($M_{bc} > 5.27 \text{ GeV}/c^2$ and $0.15 < |\Delta E| < 0.3 \text{ GeV}$). The normalization of the secondary or fake lepton background is found from the data by fitting the electron (muon) momentum distribution p_ℓ^* [29] in the B meson rest frame in the range from 0.3 to 2.4 GeV/c (0.6 to 2.4 GeV/c). The $X_u \ell \nu$ component is normalized to the number of B^+ (B^0) tags, assuming a branching fraction of 2.08×10^{-3} (1.92×10^{-3}) for $B^+ \rightarrow X_u^0 \ell^+ \nu$ ($B^0 \rightarrow X_u^- \ell^+ \nu$) [30].

The background in the M_X^2 spectrum is estimated separately in the four sub-samples, defined by the charge of B_{tag} (B^+ , B^0) and the lepton type (electron, muon).

The purity of the $B \rightarrow X_c \ell \nu$ signal depends on the sub-sample and the lepton energy threshold, typical values being around 75%. Table I shows the numbers of signal events and purities for each combination of B_{tag} charge, lepton type and lepton energy threshold.

TABLE I: Number of $B \rightarrow X_c \ell \nu$ signal candidates and signal purity in the four sub-samples, as a function of the lepton energy threshold. The yields are quoted with their statistical uncertainty; the corresponding signal purity is given in parentheses.

| E_{\min}^* | B^+ electron | B^+ muon | B^0 electron | B^0 muon |
|--------------|------------------------|------------------------|-----------------------|-----------------------|
| 0.7 | 4105 \pm 100 (70.5%) | 3739 \pm 108 (61.5%) | 2491 \pm 80 (65.9%) | 2400 \pm 86 (60.3%) |
| 0.9 | 3855 \pm 95 (73.2%) | 3591 \pm 104 (64.8%) | 2353 \pm 76 (73.4%) | 2307 \pm 83 (67.3%) |
| 1.1 | 3466 \pm 86 (74.9%) | 3305 \pm 96 (68.3%) | 2098 \pm 68 (77.1%) | 2120 \pm 76 (74.2%) |
| 1.3 | 2894 \pm 72 (75.8%) | 2857 \pm 84 (70.6%) | 1749 \pm 58 (80.4%) | 1800 \pm 66 (78.0%) |
| 1.5 | 2195 \pm 56 (74.6%) | 2225 \pm 66 (72.3%) | 1322 \pm 45 (84.2%) | 1388 \pm 52 (79.7%) |
| 1.7 | 1384 \pm 38 (77.2%) | 1415 \pm 44 (72.4%) | 824 \pm 30 (83.7%) | 878 \pm 34 (80.7%) |
| 1.9 | 571 \pm 19 (73.8%) | 627 \pm 22 (74.0%) | 353 \pm 15 (84.3%) | 376 \pm 17 (76.7%) |

F. Unfolding and Moment Calculation

We measure the M_X^2 spectrum in 45 bins in the range from 0 to 15 GeV^2/c^4 (bin width 0.333 GeV^2/c^4), which is shown in Fig. 2, and unfold the finite detector resolution in this distribution using the Singular Value Decomposition (SVD) algorithm [11]. The unfolded M_X^2 spectrum has 15 bins in the range from M_D^2 to about 15 GeV^2/c^4 . The bin width is 1 GeV^2/c^4 , except around the narrow states – D , D^* , D_1 and D_2^* – where smaller bin sizes are chosen.

The unfolding is done separately in each sub-sample (B^+ electron, B^+ muon, B^0 electron and B^0 muon). From the unfolded spectrum, we calculate the first moment and its statistical uncertainty squared,

$$\langle M_X^2 \rangle = \frac{\sum_i (M_X^2)_i x'_i}{\sum_i x'_i}, \quad \sigma^2(\langle M_X^2 \rangle) = \frac{\sum_{i,j} (M_X^2)_i X_{ij} (M_X^2)_j}{(\sum_i x'_i)^2}. \quad (3)$$

Here, x' is the unfolded spectrum corrected for slightly different bin-to-bin efficiencies and X is its covariance matrix, also determined by the SVD algorithm. $(M_X^2)_i$ is the central value of the i -th bin of the unfolded spectrum. The second central and non-central moments, $\langle (M_X^2 - \langle M_X^2 \rangle)^2 \rangle$ and $\langle M_X^4 \rangle$ are calculated from the same spectrum, substituting M_X^2 by $(M_X^2 - \langle M_X^2 \rangle)^2$ and M_X^4 in Eq. 3, respectively.

As the hadron mass moments are not expected to depend on the B meson charge or the lepton type [3, 5], we take the average over the four sub-sample results.

We have tested the entire measurement procedure including event reconstruction, unfolding and moment calculation on MC simulated events and no significant bias has been observed over the full range of lepton energy thresholds.

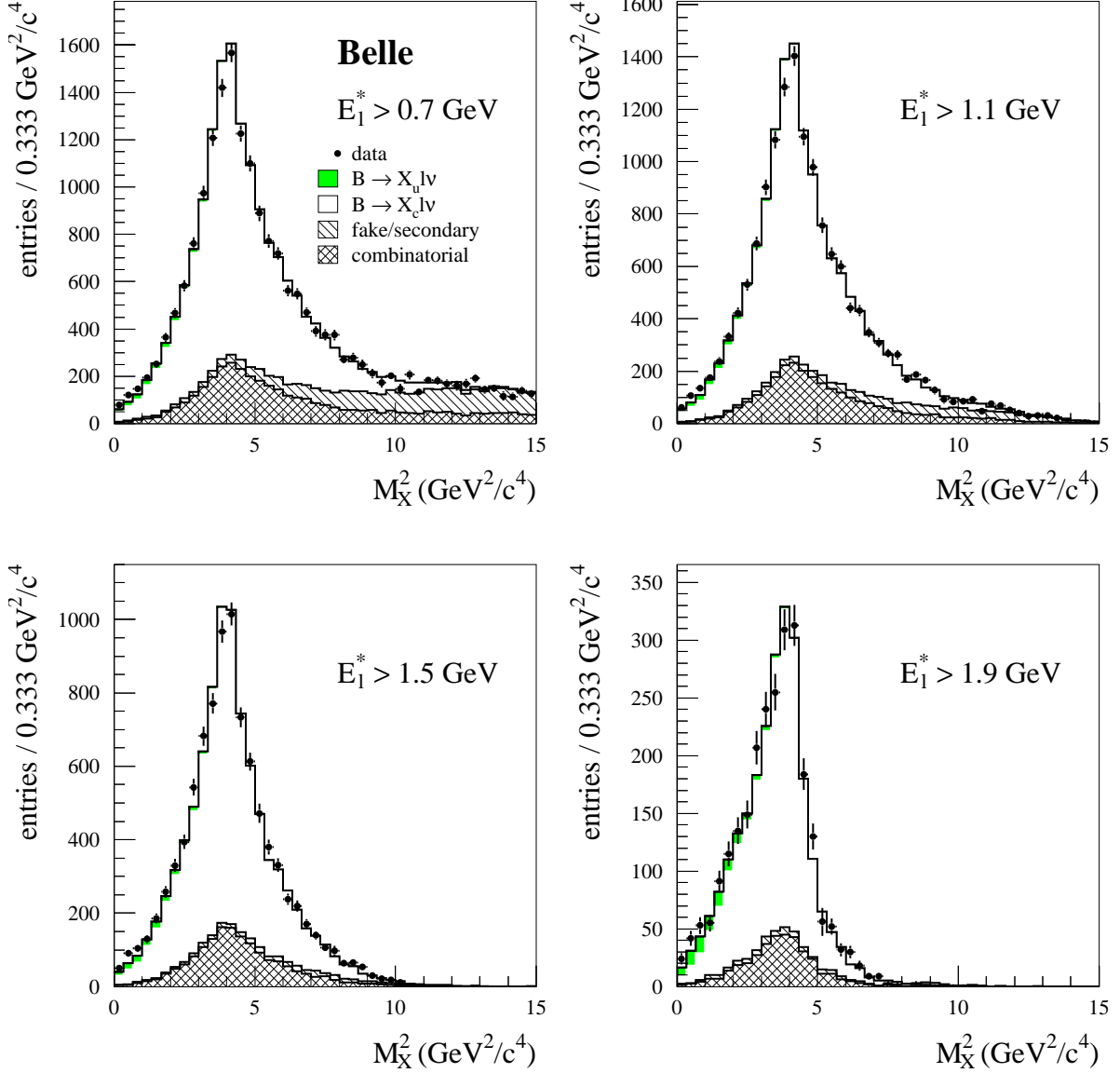


FIG. 2: Measured hadronic mass spectrum for different lepton energy thresholds. The points with error bars are the experimental data after subtraction of the continuum background. The histograms show the $B \rightarrow X_c \ell \nu$ signal and the different background components, explained in more detail in the text.

III. RESULTS AND SYSTEMATIC UNCERTAINTIES

A. Results

Our measurements of $\langle M_X^2 \rangle$, $\langle (M_X^2 - \langle M_X^2 \rangle)^2 \rangle$ and $\langle M_X^4 \rangle$ for different lepton energy thresholds are shown in Table II and Fig. 3. The sub-sample results for a given charge of B_{tag} (B^+ , B^0) or lepton type (electron, muon) are compatible within their statistical uncertainty only.

TABLE II: Measurements of $\langle M_X^2 \rangle$, $\langle (M_X^2 - \langle M_X^2 \rangle)^2 \rangle$ and $\langle M_X^4 \rangle$ for different lepton energy thresholds. The results in this table are the averages of the four sub-samples, defined by the charge of B_{tag} (B^+ , B^0) and the lepton type (electron, muon). The first error is statistical, the second is the estimated systematic uncertainty. The different measurements are highly correlated (Tables VI–X).

| E_{min}^* (GeV) | $\langle M_X^2 \rangle$ (GeV ² /c ⁴) | $\langle (M_X^2 - \langle M_X^2 \rangle)^2 \rangle$ (GeV ⁴ /c ⁸) | $\langle M_X^4 \rangle$ (GeV ⁴ /c ⁸) |
|--------------------------|---|---|---|
| 0.7 | 4.403 ± 0.036 ± 0.052 | 1.494 ± 0.173 ± 0.327 | 20.88 ± 0.48 ± 0.77 |
| 0.9 | 4.353 ± 0.032 ± 0.041 | 1.229 ± 0.138 ± 0.244 | 20.18 ± 0.40 ± 0.58 |
| 1.1 | 4.293 ± 0.028 ± 0.029 | 0.940 ± 0.098 ± 0.137 | 19.37 ± 0.33 ± 0.36 |
| 1.3 | 4.213 ± 0.027 ± 0.024 | 0.641 ± 0.071 ± 0.080 | 18.40 ± 0.29 ± 0.26 |
| 1.5 | 4.144 ± 0.028 ± 0.022 | 0.515 ± 0.061 ± 0.064 | 17.69 ± 0.28 ± 0.23 |
| 1.7 | 4.056 ± 0.033 ± 0.022 | 0.322 ± 0.058 ± 0.040 | 16.77 ± 0.32 ± 0.21 |
| 1.9 | 3.996 ± 0.041 ± 0.021 | 0.143 ± 0.056 ± 0.038 | 16.11 ± 0.38 ± 0.20 |

TABLE III: Breakup of the systematic error on $\langle M_X^2 \rangle$. Refer to the text for details.

| E_{min}^* (GeV) | $\Delta \langle M_X^2 \rangle$ (GeV ² /c ⁴) | | | | | | |
|---|--|-------|-------|-------|-------|-------|-------|
| | 0.7 | 0.9 | 1.1 | 1.3 | 1.5 | 1.7 | 1.9 |
| secondary/fake leptons | 0.033 | 0.023 | 0.013 | 0.007 | 0.004 | 0.002 | 0.000 |
| combinatorial background | 0.006 | 0.004 | 0.003 | 0.002 | 0.002 | 0.002 | 0.000 |
| continuum | 0.000 | 0.000 | 0.000 | 0.000 | 0.000 | 0.000 | 0.000 |
| $B \rightarrow X_u \ell \nu$ background | 0.004 | 0.004 | 0.004 | 0.004 | 0.006 | 0.007 | 0.009 |
| $\mathcal{B}(D^{(*)} \ell \nu)$ | 0.008 | 0.007 | 0.007 | 0.007 | 0.006 | 0.005 | 0.003 |
| $\mathcal{B}(D^{**} \ell \nu)$ | 0.022 | 0.014 | 0.006 | 0.000 | 0.000 | 0.008 | 0.006 |
| $\mathcal{B}((D^{(*)} \pi)_{\text{non-res.}} \ell \nu)$ | 0.024 | 0.017 | 0.007 | 0.004 | 0.004 | 0.004 | 0.004 |
| $D^{(*)} \ell \nu$ form factors | 0.013 | 0.013 | 0.012 | 0.011 | 0.010 | 0.008 | 0.006 |
| $D^{**} \ell \nu$ form factors | 0.003 | 0.002 | 0.002 | 0.001 | 0.001 | 0.001 | 0.004 |
| unfolding | 0.015 | 0.015 | 0.015 | 0.015 | 0.015 | 0.015 | 0.015 |
| binning | 0.001 | 0.001 | 0.001 | 0.001 | 0.001 | 0.000 | 0.001 |
| efficiency | 0.008 | 0.011 | 0.012 | 0.009 | 0.008 | 0.005 | 0.004 |
| total | 0.052 | 0.041 | 0.029 | 0.024 | 0.022 | 0.022 | 0.021 |

B. Systematic Uncertainties

The different contributions to the systematic error are shown in Tables III–V. The total systematic error in Table II corresponds to the quadratic sum of these components.

The uncertainties related to the different background components in M_X^2 are estimated by varying the respective background normalization factors within ± 1 standard deviation.

We consider both variations of the $B \rightarrow D^{(*)} \ell \nu$ branching fractions and form factor

TABLE IV: Same as Table III for $\langle(M_X^2 - \langle M_X^2 \rangle)^2\rangle$.

| E_{\min}^* (GeV) | $\Delta\langle(M_X^2 - \langle M_X^2 \rangle)^2\rangle$ (GeV ⁴ /c ⁸) | | | | | | |
|---|---|-------|-------|-------|-------|-------|-------|
| | 0.7 | 0.9 | 1.1 | 1.3 | 1.5 | 1.7 | 1.9 |
| secondary/fake leptons | 0.167 | 0.109 | 0.050 | 0.023 | 0.009 | 0.005 | 0.002 |
| combinatorial background | 0.028 | 0.018 | 0.009 | 0.005 | 0.003 | 0.002 | 0.001 |
| continuum | 0.000 | 0.000 | 0.000 | 0.000 | 0.000 | 0.001 | 0.000 |
| $B \rightarrow X_u \ell \nu$ background | 0.004 | 0.004 | 0.004 | 0.003 | 0.003 | 0.005 | 0.005 |
| $\mathcal{B}(D^{(*)} \ell \nu)$ | 0.013 | 0.010 | 0.007 | 0.004 | 0.002 | 0.002 | 0.003 |
| $\mathcal{B}(D^{**} \ell \nu)$ | 0.216 | 0.169 | 0.102 | 0.049 | 0.042 | 0.011 | 0.009 |
| $\mathcal{B}((D^{(*)} \pi)_{\text{non-res.}} \ell \nu)$ | 0.168 | 0.125 | 0.058 | 0.041 | 0.024 | 0.004 | 0.004 |
| $D^{(*)} \ell \nu$ form factors | 0.029 | 0.028 | 0.024 | 0.019 | 0.017 | 0.016 | 0.007 |
| $D^{**} \ell \nu$ form factors | 0.013 | 0.009 | 0.006 | 0.003 | 0.004 | 0.001 | 0.004 |
| unfolding | 0.035 | 0.035 | 0.035 | 0.035 | 0.035 | 0.035 | 0.035 |
| binning | 0.001 | 0.001 | 0.000 | 0.001 | 0.001 | 0.001 | 0.002 |
| efficiency | 0.025 | 0.032 | 0.027 | 0.014 | 0.013 | 0.005 | 0.002 |
| total | 0.327 | 0.244 | 0.137 | 0.080 | 0.064 | 0.040 | 0.038 |

 TABLE V: Same as Table III for $\langle M_X^4 \rangle$.

| E_{\min}^* (GeV) | $\Delta\langle M_X^4 \rangle$ (GeV ⁴ /c ⁸) | | | | | | |
|---|---|------|------|------|------|------|------|
| | 0.7 | 0.9 | 1.1 | 1.3 | 1.5 | 1.7 | 1.9 |
| secondary/fake leptons | 0.46 | 0.31 | 0.16 | 0.09 | 0.04 | 0.02 | 0.00 |
| combinatorial background | 0.08 | 0.05 | 0.04 | 0.03 | 0.01 | 0.01 | 0.00 |
| continuum | 0.00 | 0.00 | 0.00 | 0.00 | 0.00 | 0.00 | 0.00 |
| $B \rightarrow X_u \ell \nu$ background | 0.04 | 0.04 | 0.04 | 0.04 | 0.05 | 0.06 | 0.07 |
| $\mathcal{B}(D^{(*)} \ell \nu)$ | 0.07 | 0.07 | 0.06 | 0.05 | 0.04 | 0.03 | 0.02 |
| $\mathcal{B}(D^{**} \ell \nu)$ | 0.41 | 0.30 | 0.14 | 0.04 | 0.04 | 0.05 | 0.06 |
| $\mathcal{B}((D^{(*)} \pi)_{\text{non-res.}} \ell \nu)$ | 0.38 | 0.28 | 0.12 | 0.08 | 0.06 | 0.04 | 0.04 |
| $D^{(*)} \ell \nu$ form factors | 0.15 | 0.14 | 0.13 | 0.12 | 0.10 | 0.09 | 0.04 |
| $D^{**} \ell \nu$ form factors | 0.04 | 0.03 | 0.02 | 0.01 | 0.01 | 0.00 | 0.03 |
| unfolding | 0.16 | 0.16 | 0.16 | 0.16 | 0.16 | 0.16 | 0.16 |
| binning | 0.01 | 0.01 | 0.01 | 0.00 | 0.00 | 0.01 | 0.00 |
| efficiency | 0.09 | 0.13 | 0.13 | 0.09 | 0.08 | 0.04 | 0.03 |
| total | 0.77 | 0.58 | 0.36 | 0.26 | 0.23 | 0.21 | 0.20 |

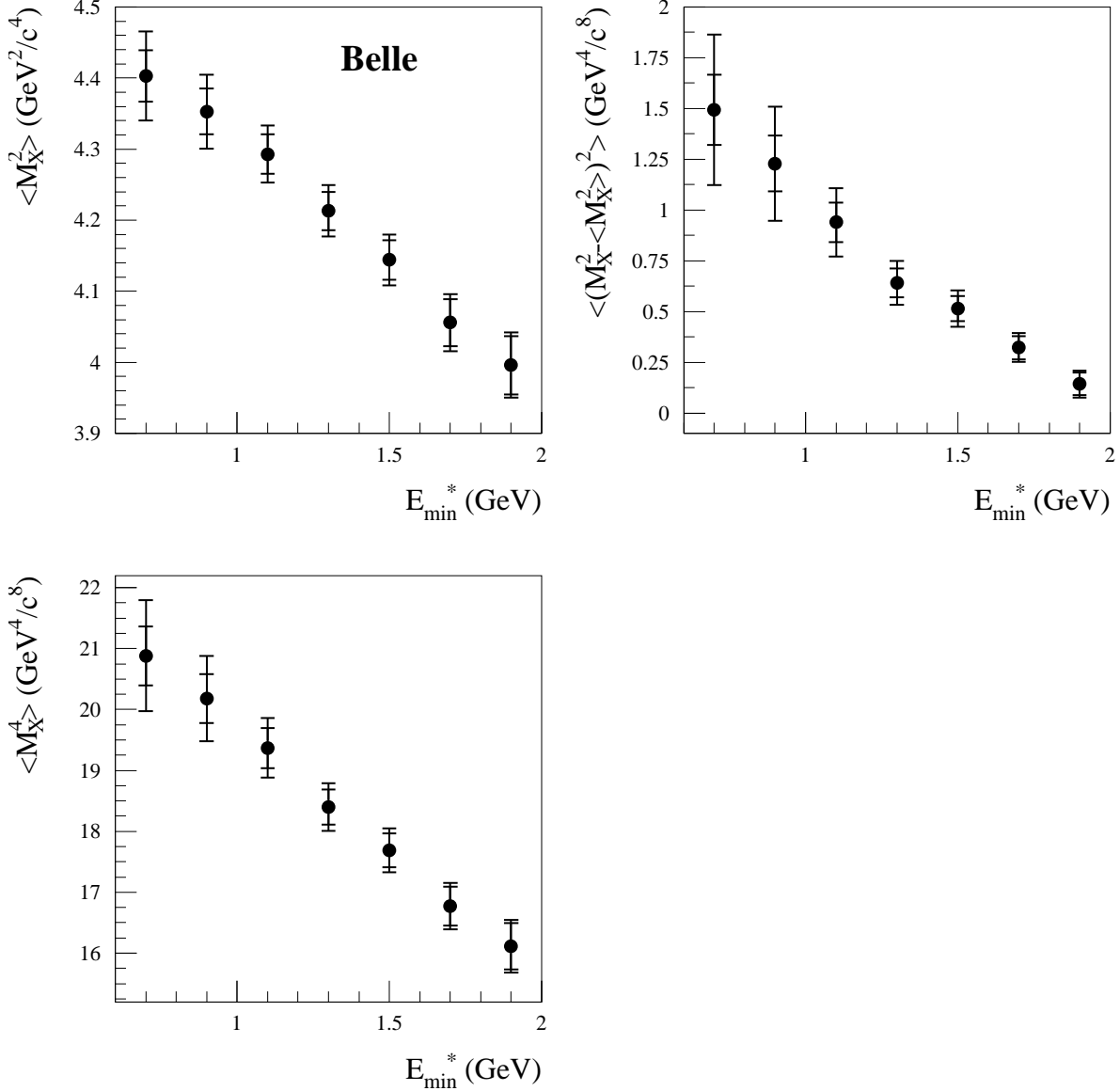


FIG. 3: Graphical representation of the results in Table II. The error bars indicate the statistical and total experimental errors.

shapes. For the former, the ranges of variation are taken from Ref. [31]. For the latter, the curvature ρ^2 in the form factor parametrization [16] is varied within 1.56 ± 0.14 (1.15 ± 0.16) for $B \rightarrow D^* \ell \nu$ ($B \rightarrow D \ell \nu$) [32]. For $B \rightarrow D^* \ell \nu$, we also vary the form factor ratios R_1 and R_2 [33].

The LLSW model [18] predicts the relative abundance and the form factor shape of the different components in $B \rightarrow D^{**} \ell \nu$ only. To obtain the absolute branching fractions of the $B \rightarrow D^{**} \ell \nu$ components and of $B \rightarrow (D^{(*)} \pi)_{\text{non-res.}} \ell \nu$, we use $\mathcal{B}(B^+ \rightarrow \bar{D}_1^0 \ell^+ \nu) = (5.6 \pm 1.6) \times 10^{-3}$ [31], the recent Belle measurement of $\mathcal{B}(B \rightarrow D^{(*)} \pi \ell \nu)$ [34] and the total semileptonic branching fraction [31]. The uncertainty assigned to the $B \rightarrow D^{**} \ell \nu$ branching fractions in Tables III–V reflects the uncertainty in these measurements and the change in the $B \rightarrow D^{**} \ell \nu$ composition when varying the LLSW parameters within their allowed range.

TABLE VI: Correlation coefficients between $\langle M_X^2 \rangle$ measurements.

| E_{\min}^* (GeV) | $\langle M_X^2 \rangle$ | | | | | | |
|-----------------------------|-------------------------|-------|-------|-------|-------|-------|-------|
| | 0.7 | 0.9 | 1.1 | 1.3 | 1.5 | 1.7 | 1.9 |
| 0.7 | 1.000 | 0.932 | 0.786 | 0.615 | 0.481 | 0.168 | 0.071 |
| 0.9 | | 1.000 | 0.888 | 0.715 | 0.573 | 0.241 | 0.116 |
| 1.1 | | | 1.000 | 0.849 | 0.693 | 0.363 | 0.194 |
| $\langle M_X^2 \rangle$ 1.3 | | | | 1.000 | 0.804 | 0.470 | 0.254 |
| 1.5 | | | | | 1.000 | 0.591 | 0.308 |
| 1.7 | | | | | | 1.000 | 0.363 |
| 1.9 | | | | | | | 1.000 |

 TABLE VII: Correlation coefficients between $\langle M_X^2 \rangle$ and $\langle (M_X^2 - \langle M_X^2 \rangle)^2 \rangle$ measurements.

| E_{\min}^* (GeV) | $\langle (M_X^2 - \langle M_X^2 \rangle)^2 \rangle$ | | | | | | |
|-----------------------------|---|-------|-------|-------|-------|-------|-------|
| | 0.7 | 0.9 | 1.1 | 1.3 | 1.5 | 1.7 | 1.9 |
| 0.7 | 0.897 | 0.847 | 0.788 | 0.713 | 0.576 | 0.306 | 0.102 |
| 0.9 | 0.777 | 0.843 | 0.804 | 0.726 | 0.608 | 0.356 | 0.144 |
| 1.1 | 0.548 | 0.615 | 0.757 | 0.690 | 0.606 | 0.426 | 0.211 |
| $\langle M_X^2 \rangle$ 1.3 | 0.328 | 0.371 | 0.483 | 0.718 | 0.599 | 0.476 | 0.260 |
| 1.5 | 0.223 | 0.263 | 0.346 | 0.481 | 0.702 | 0.559 | 0.280 |
| 1.7 | -.051 | -.031 | 0.035 | 0.126 | 0.237 | 0.846 | 0.296 |
| 1.9 | -.060 | -.047 | -.007 | 0.040 | 0.075 | 0.228 | 0.865 |

The SVD algorithm used to unfold the measured M_X^2 distribution requires the detector response matrix, *i.e.*, the distribution of measured versus true values of M_X^2 . We determine this matrix from the MC simulation. To study the systematics related to unfolding and a possible mismodeling of the detector response, we change the amount of bin-to-bin migration by varying the effective rank of the detector response matrix, the main tunable parameter of the SVD algorithm. We have further studied a change of the binning of the unfolded distribution and the effect of disabling the bin-to-bin efficiency correction.

C. Correlations

Due to overlapping events, the moment measurements corresponding to different lepton energy thresholds are highly correlated. Systematic uncertainties are another source of correlation. We have estimated the correlations due to both sources using a toy MC approach based on 50,000 simulated measurements. The results for the self- and cross-correlation coefficients are given in Tables VI–X.

TABLE VIII: Correlation coefficients between $\langle M_X^2 \rangle$ and $\langle M_X^4 \rangle$ measurements.

| E_{\min}^* (GeV) | $\langle M_X^4 \rangle$ | | | | | | |
|-----------------------------|-------------------------|-------|-------|-------|-------|-------|-------|
| | 0.7 | 0.9 | 1.1 | 1.3 | 1.5 | 1.7 | 1.9 |
| 0.7 | 0.983 | 0.933 | 0.830 | 0.683 | 0.523 | 0.194 | 0.073 |
| 0.9 | 0.890 | 0.974 | 0.910 | 0.765 | 0.606 | 0.264 | 0.117 |
| 1.1 | 0.704 | 0.810 | 0.976 | 0.857 | 0.707 | 0.380 | 0.196 |
| $\langle M_X^2 \rangle$ 1.3 | 0.508 | 0.601 | 0.774 | 0.980 | 0.800 | 0.479 | 0.258 |
| 1.5 | 0.383 | 0.469 | 0.614 | 0.764 | 0.985 | 0.597 | 0.305 |
| 1.7 | 0.079 | 0.137 | 0.273 | 0.403 | 0.539 | 0.994 | 0.357 |
| 1.9 | 0.017 | 0.052 | 0.136 | 0.208 | 0.271 | 0.348 | 0.995 |

 TABLE IX: Correlation coefficients between $\langle (M_X^2 - \langle M_X^2 \rangle)^2 \rangle$ measurements.

| E_{\min}^* (GeV) | $\langle (M_X^2 - \langle M_X^2 \rangle)^2 \rangle$ | | | | | | |
|---|---|-------|-------|-------|-------|-------|-------|
| | 0.7 | 0.9 | 1.1 | 1.3 | 1.5 | 1.7 | 1.9 |
| 0.7 | 1.000 | 0.939 | 0.838 | 0.698 | 0.534 | 0.167 | -.024 |
| 0.9 | | 1.000 | 0.901 | 0.732 | 0.586 | 0.195 | -.011 |
| $\langle (M_X^2 - \langle M_X^2 \rangle)^2 \rangle$ 1.1 | | | 1.000 | 0.793 | 0.638 | 0.262 | 0.034 |
| 1.3 | | | | 1.000 | 0.731 | 0.340 | 0.102 |
| 1.5 | | | | | 1.000 | 0.484 | 0.146 |
| 1.7 | | | | | | 1.000 | 0.296 |
| 1.9 | | | | | | | 1.000 |

 TABLE X: Correlation coefficients between $\langle M_X^4 \rangle$ measurements.

| E_{\min}^* (GeV) | $\langle M_X^4 \rangle$ | | | | | | |
|-----------------------------|-------------------------|-------|-------|-------|-------|-------|-------|
| | 0.7 | 0.9 | 1.1 | 1.3 | 1.5 | 1.7 | 1.9 |
| 0.7 | 1.000 | 0.932 | 0.784 | 0.601 | 0.442 | 0.111 | 0.017 |
| 0.9 | | 1.000 | 0.877 | 0.684 | 0.524 | 0.168 | 0.051 |
| 1.1 | | | 1.000 | 0.817 | 0.651 | 0.297 | 0.137 |
| $\langle M_X^4 \rangle$ 1.3 | | | | 1.000 | 0.780 | 0.421 | 0.212 |
| 1.5 | | | | | 1.000 | 0.557 | 0.270 |
| 1.7 | | | | | | 1.000 | 0.346 |
| 1.9 | | | | | | | 1.000 |

IV. SUMMARY

We have measured the first, $\langle M_X^2 \rangle$, and the second central and non-central moments, $\langle (M_X^2 - \langle M_X^2 \rangle)^2 \rangle$ and $\langle M_X^4 \rangle$, of the hadronic mass squared spectrum in $B \rightarrow X_c \ell \nu$ decays for lepton energy thresholds ranging from 0.7 to 1.9 GeV. Using a toy MC approach, we have also evaluated the full covariance matrix for this set of measurements.

It is expected that this measurement, combined with measurements of the semileptonic branching fraction, moments of the lepton energy spectrum in $B \rightarrow X_c \ell \nu$ decays and possibly other moments, will lead to an improved determination of b -quark mass m_b and the CKM matrix element $|V_{cb}|$ [2, 3, 4, 5].

Acknowledgments

We thank the KEKB group for the excellent operation of the accelerator, the KEK cryogenics group for the efficient operation of the solenoid, and the KEK computer group and the National Institute of Informatics for valuable computing and Super-SINET network support. We acknowledge support from the Ministry of Education, Culture, Sports, Science, and Technology of Japan and the Japan Society for the Promotion of Science; the Australian Research Council and the Australian Department of Education, Science and Training; the National Science Foundation of China and the Knowledge Innovation Program of the Chinese Academy of Sciences under contract No. 10575109 and IHEP-U-503; the Department of Science and Technology of India; the BK21 program of the Ministry of Education of Korea, the CHEP SRC program and Basic Research program (grant No. R01-2005-000-10089-0) of the Korea Science and Engineering Foundation, the Pure Basic Research Group program of the Korea Research Foundation, and the SBS Foundation; the Polish State Committee for Scientific Research; the Ministry of Science and Technology of the Russian Federation; the Slovenian Research Agency; the Swiss National Science Foundation; the National Science Council and the Ministry of Education of Taiwan; and the U.S. Department of Energy.

-
- [1] N. Cabibbo, Phys. Rev. Lett. **10**, 531 (1963);
M. Kobayashi and T. Maskawa, Prog. Theor. Phys. **49**, 652 (1973).
 - [2] D. Benson, I. I. Bigi, T. Mannel and N. Uraltsev, Nucl. Phys. B **665**, 367 (2003) [hep-ph/0302262].
 - [3] P. Gambino and N. Uraltsev, Eur. Phys. J. C **34**, 181 (2004) [hep-ph/0401063].
 - [4] D. Benson, I. I. Bigi and N. Uraltsev, Nucl. Phys. B **710**, 371 (2005) [hep-ph/0410080].
 - [5] C. W. Bauer, Z. Ligeti, M. Luke and A. V. Manohar, Phys. Rev. D **67**, 054012 (2003) [hep-ph/0210027].
 - [6] B. Aubert *et al.* [BABAR Collaboration], Phys. Rev. D **69**, 111103 (2004) [hep-ex/0403031].
 - [7] S. E. Csorna *et al.* [CLEO Collaboration], Phys. Rev. D **70**, 032002 (2004) [hep-ex/0403052].
 - [8] D. Acosta *et al.* [CDF Collaboration], Phys. Rev. D **71**, 051103 (2005) [hep-ex/0502003].
 - [9] J. Abdallah *et al.* [DELPHI Collaboration], Eur. Phys. J. C **45**, 35 (2006) [hep-ex/0510024].
 - [10] We provide numbers for both definitions of the second moment, $\langle (M_X^2 - \langle M_X^2 \rangle)^2 \rangle$ and $\langle M_X^4 \rangle$, used in literature [3, 5] for the convenience of further applications though one can be derived from the other.

- [11] A. Höcker and V. Kartvelishvili, Nucl. Instrum. Meth. A **372**, 469 (1996) [hep-ph/9509307].
- [12] A. Abashian *et al.* [Belle Collaboration], Nucl. Instrum. Meth. A **479**, 117 (2002).
- [13] S. Kurokawa, Nucl. Instrum. Meth. A **499**, 1 (2003), and other papers included in this volume.
- [14] D. J. Lange, Nucl. Instrum. Meth. A **462**, 152 (2001).
- [15] R. Brun, F. Bruyant, M. Maire, A. C. McPherson and P. Zancarini, CERN-DD/EE/84-1.
- [16] I. Caprini, L. Lellouch and M. Neubert, Nucl. Phys. B **530**, 153 (1998) [hep-ph/9712417].
- [17] In this paper, the symbol D^{**} refers collectively to the D_1 , D_2^* , D_0^* and D_1' states.
- [18] A. K. Leibovich, Z. Ligeti, I. W. Stewart and M. B. Wise, Phys. Rev. D **57**, 308 (1998) [hep-ph/9705467].
- [19] J. L. Goity and W. Roberts, Phys. Rev. D **51**, 3459 (1995) [hep-ph/9406236].
- [20] F. De Fazio and M. Neubert, JHEP **9906**, 017 (1999) [hep-ph/9905351].
- [21] P. Ball and V. M. Braun, Phys. Rev. D **58**, 094016 (1998) [hep-ph/9805422].
- [22] P. Ball and R. Zwicky, JHEP **0110**, 019 (2001) [hep-ph/0110115].
- [23] D. Scora and N. Isgur, Phys. Rev. D **52**, 2783 (1995) [hep-ph/9503486].
- [24] E. Barberio and Z. Was, Comput. Phys. Commun. **79**, 291 (1994).
- [25] K. Abe *et al.* [Belle Collaboration], Phys. Rev. D **64**, 072001 (2001) [hep-ex/0103041].
- [26] In this paper, the inclusion of the charge conjugate decay is implied.
- [27] K. Hanagaki, H. Kakuno, H. Ikeda, T. Iijima and T. Tsukamoto, Nucl. Instrum. Meth. A **485**, 490 (2002) [hep-ex/0108044].
- [28] A. Abashian *et al.*, Nucl. Instrum. Meth. A **491**, 69 (2002).
- [29] In this paper, quantities calculated in the B meson rest frame are denoted by an asterisk.
- [30] These numbers are our private averages of $B \rightarrow X_u \ell \nu$ measurements by LEP, CLEO, BaBar and Belle. The uncertainty in these branching fractions is assumed to be 20%.
- [31] W. M. Yao *et al.* [Particle Data Group], J. Phys. G **33**, 1 (2006).
- [32] E. Barberio *et al.* [Heavy Flavor Averaging Group (HFAG)], hep-ex/0603003.
- [33] B. Aubert *et al.* [BABAR Collaboration], hep-ex/0602023.
- [34] D. Liventsev *et al.*, Phys. Rev. D **72**, 051109 (2005).